Biochemistry

 Volume 42, Number 36 September 16, 2003

*Accelerated Publications*

# Do Enzymes Change the Nature of Transition States? Mapping the Transition State for General Acid−Base Catalysis of a Serine Protease‡

Richard R. Bott, Gina Chan, Blanca Domingo, Grant Ganshaw, Constance Y. Hsia,§ Mark Knapp,|| and Christopher J. Murray*

*Department of Molecular Evolution and Design, Genencor International, Incorporated, 925 Page Mill Road, Palo Alto, California 94304*

*Received May 13, 2003; Revised Manuscript Received June 19, 2003*

ABSTRACT: The properties of the transition state for serine protease-catalyzed hydrolysis of an amide bond were determined for a series of subtilisin variants from *Bacillus lentus*. There is no significant change in the structure of the enzyme upon introduction of charged mutations S156E/S166D, suggesting that changes in catalytic activity reflect global properties of the enzyme. The effect of charged mutations on the p$K_a$ of the active site histidine-64 $N^{\epsilon 2}$-H was correlated with changes in the second-order rate constant $k_{cat}/K_m$ for hydrolysis of tetrapeptide anilides at low ionic strength with a Brønsted slope $\alpha = 1.1$. The solvent isotope effect $^{D_2O}(k_{cat}/K_m)_1 = 1.4 \pm 0.2$. These results are consistent with a rate-limiting breakdown of the tetrahedral intermediate in the acylation step with hydrogen bond stabilization of the departing amine leaving group. There is an increase in the ratio of hydrolysis of succinyl-Ala-Ala-Pro-Phe-anilides for *p*-nitroaniline versus aniline leaving groups with variants with more basic active site histidines that can be described by the interaction coefficient $p_{xy} = \partial\beta_{lg}/\partial pK_a$ (H64) = 0.15. This is attributed to increased hydrogen bonding of the active site imidazolium N−H to the more basic amine leaving group as well as electrostatic destabilization of the transition state. A qualitative characterization of the transition state is presented in terms of a reaction coordinate diagram that is defined by the structure−reactivity parameters.

Since the early demonstration of enzyme specificity by Fischer (*1*), there have been many attempts to provide quantitative descriptions of the mechanisms of enzymatic rate enhancements. Serine proteases have served prominently as a paradigm for understanding these mechanisms and the relationship between enzyme structure and function. For example, general acid−base catalysis by active site acids and bases is a common mechanism for stabilizing the transition state of protease- (*2*−*4*), isomerase- (*5*), transaminase- (*6*), and glycosidase-catalyzed (*7*) reactions. We would like to understand the transition state structures for these reactions in terms of the dynamics (*8*, *9*) and ultrahigh-resolution structures (*10*) of enzymes. A related question is whether these transition state structures differ significantly from the corresponding nonenzymatic reactions in solution (*11*−*13*).

Measures of the reaction progress or bond order in the transition state can be determined from kinetic isotope effects

‡ Atomic coordinates for the S156E/S166D subtilisin variant described in this paper have been deposited in the RCSB Protein Data Bank (http://www.rcsb.org) under the accession code 1Q5P.

* To whom correspondence should be addressed. Phone: (650) 846-5861. Fax: (650) 845-5809. E-mail: cmurray@genencor.com.

§ Present address: Weill Medical College of Cornell University, 515 East 71st St., Room S-222, New York, NY 10021.

|| Present address: Roche Biosciences, 3431 Hillview Ave., Palo Alto, CA 94304-1397.

10.1021/bi034773m CCC: $25.00 
Published on Web 08/19/2003

Scheme 1

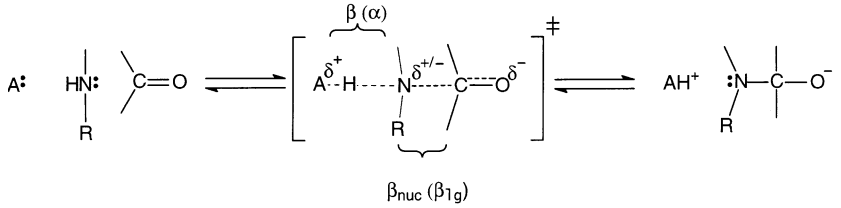


or structure−reactivity coefficients such as Brønsted slopes $\alpha$ for proton transfer or $\beta_{lg}$ for bond breaking. General acid−base-catalyzed reactions in water often show a linear free energy relationship (LFER)[1] between log $k$ for a series of catalysts and the corresponding p$K_a$ of the catalyst as described by eq 1 (*14*, *15*).

$$\log k = \alpha \mathrm{p}K_a + C \quad (1)$$

The slope $\alpha$ (or $\beta$ value) provides a crude measure of the degree of proton transfer or the amount of charge developed in the transition state.

The application of LFERs to enzymes is frequently limited due to rate-determining conformational or diffusion steps, the extreme specificity requirements of enzymes, and other factors (*3*, *16*−*18*). One approach that avoids some of these problems uses chemical rescue of enzyme variants by a homologous series of exogenous bases to probe mechanisms of enzyme-catalyzed reactions (*6*). In any event, it is necessary to establish unambiguously the rate-limiting step measured in the enzyme reaction before any mechanistic interpretation of changes in reactivity with changes in p$K_a$ of the catalyst or leaving group can be made. We are interested here in the question of whether changes in reactivity introduced by changes in the structure of an enzyme can be interpreted similarly to slopes (and changes in slopes) of LFERs in corresponding nonenzyme-catalyzed reactions.

Slopes of LFERs are first derivatives of log $k$. However, these slopes are not always constant. Changes in the Brønsted slope defined for a series of acids or bases can occur when the solvent is changed or when a substituent is changed in the other reactant as illustrated for acyl transfer reactions involving the formation (or breakdown in the reverse direction) of a tetrahedral intermediate, catalyzed by general bases A: in water (Scheme 1).

An empirical approach toward characterizing transition state structure is based on changes in Brønsted slopes with changes in structure that can be described by interaction coefficients introduced by Jencks (*19*) and others. Interaction coefficients provide a measure of the relative contributions, or coupling, between bond-making and -breaking processes in the transition state for reactions such as Scheme 1 where multiple bonding changes occur. It may be easier to evaluate changes in the transition state structure from interaction coefficients since steric, electrostatic, and hydrophobic effects that influence the slope of a Brønsted plot will tend to cancel. This may be especially important in the complicated environment of an enzyme active site.

Using LFERs we report here evidence that the transition state structure for a serine protease-catalyzed hydrolysis of an amide bond shows significant coupling between the proton donated by the catalytic histidine residue that forms part of the Asp-His-Ser catalytic triad and the nitrogen of the amine leaving group. Subtilisin from *Bacillus lentus*[2] was engineered to alter the p$K_a$ of the active site His-64 by remote electrostatic effects. Kinetic data for the hydrolysis of tetrapeptide anilide substrates by a series of subtilisin variants are consistent with a rate-limiting breakdown of the enzymatic tetrahedral intermediate in the acylation step and allow an estimate of an interaction coefficient $p_{xy} = \partial\beta_{lg}/\partial \mathrm{p}K_a = 0.15$, which describes changes in the strength of the hydrogen bond from the active site histidine to the leaving group nitrogen with changes in the p$K_a$ of His-64. The changes in transition state structure introduced by site-directed mutations near the active site histidine are larger than changes in transition state structure introduced by remote substituents in nonenzyme-catalyzed acyl transfer reactions in water. Additional studies of other enzymes will be required to determine the generality of this result.

## EXPERIMENTAL PROCEDURES

*Materials.* Reagent grade inorganic salts were used without further purification. Ethylenediamine•2HCl from Aldrich was recrystallized before use. *N*-Acetyl-Ala-Ala-Pro-Phe-*p*-nitroanilide (Ac-AAPF-pNA) and succinyl-AAPF-pNA were purchased from Bachem (Torrance, CA). *N*-Acetyl-Ala-Ala-Pro-Phe-anilide (ac-AAPF-anilide) and 3-fluoroanilide were from Synpep (Dublin, CA). *N*-(Carbobenzoxy)-Leu-Leu-Phe trifluoromethyl ketone (*Z*-LLF-$CF_3$) was synthesized as previously described (*20*). Variants of subtilisin from *B. lentus* were constructed by site-directed mutagenesis, expressed, and purified as previously described (*21*). Samples were stored at a concentration of 2.0 mg/mL in 50% propylene glycol at 4 °C after the determination of active site concentration and showed no loss in activity over 5 years under these conditions.

*Methods.* The crystal structure of the phenylmethylsulfonyl fluoride (PMSF) inhibited S156E/S166D variant of DSAI (DSAI accession code 1C9M) was solved to an $R_{merge}$ of 0.060 by molecular replacement using the procedures described by Graycar et al. (*9*). The space group is $P2_12_12_1$ with unit cell dimensions of $a = 53.45$ Å, $b = 61.50$ Å, and $c = 75.30$ Å. Active enzyme concentrations were determined

[1] Abbreviations: Ac-AAPF-pNA, *N*-acetyl-Ala-Ala-Pro-Phe-*p*-nitroanilide; C−N, carbon−nitrogen; DMSO, dimethyl sulfoxide; DSAI, engineered variant of *B. lentus* subtilisin N76D/N87S/S103A/V104I E•S, Michaelis enzyme substrate complex; LFER, linear free energy relationship; PMSF, phenylmethyl sulfonyl fluoride; suc-AAPF-*p*NA, *N*-succinyl-Ala-Ala-Pro-Phe-*p*-nitroanilide; TI, tetrahedral intermediate; TS, transition state; Z-LLF-$CF_3$, *N*-(carbobenzoxy)-Leu-Leu-Phe trifluoromethyl ketone.

[2] The amino acid numbering used for the subtilisin variants discussed in this paper corresponds to that of mature *Bacillus amyloliquefaciens* (subtilisin BPN′). The parent enzyme is *B. lentus* subtilisin N76D/N87S/S103A/V104I.

with a precision of ±5% by titration with phenylmethyl sulfonyl fluoride (PMSF) or mung bean inhibitor using methods described previously (*21*, *22*). First-order kinetics at 25 °C, ionic strength 0.05 M (KCl), and 0.005% Tween-20 in ethylenediamine buffers were followed using a SpectraMax 250 plate reader with 96-well polystyrene plates (Molecular Devices, Sunnyvale, CA) or an HP 8452A spectrophomoter, essentially as previously described (*23*). Substrate concentrations were $<0.1K_m$ and [DMSO] < 0.1%. The use of ethylenediamine buffers ($pK_a = 7.15$ for dication; $pK_a = 10.3$ for monocation) allowed the determination of pH rate profiles over a wide range of pH with a single buffer.

*Data Analysis*. All fits were done using Grafit 3.0 (*24*). First-order kinetic curves were fit to a single-exponential rate equation, while biphasic curves for competitive substrate hydrolysis were fitted to a two exponential rate equation (*25*). Values of $k_{cat}/K_m$ were calculated from the observed rate constant and the measured enzyme concentration according to

$$k_{cat}/K_m = k_{obs}/[E] \quad (2)$$

The pH dependence of $k_{cat}/K_m$ was fit to eq 3, where $pK_{a1}$ corresponds to the $pK_a$ of the active site histidine, $(k_{cat}/K_m)_1$ is the second-order rate constant with histidine ionized, $pK_{a2}$ refers to the ionization of Y167 (B. Domingo and C. J. Murray, unpublished), and $(k_{cat}/K_m)_2$ is the second-order rate constant for the fully ionized form of the enzyme.

$$k_{cat}/K_m = \left[\frac{(k_{cat}/K_m)_1 10^{pH-pK_{a1}}}{10^{pH-pK_{a1}}+1}\right] - \left[\frac{((k_{cat}/K_m)_1 - (k_{cat}/K_m)_2)10^{pH-pK_{a2}}}{10^{pH-pK_{a2}}+1}\right] \quad (3)$$

Michaelis-Menten parameters $k_{cat}$ and $K_m$ at pH 7.5, as well as inhibition constants $K_i$ for *Z*-LLF-$CF_3$, were measured in 50 mM potassium phosphate, 4% (v/v) DMSO by monitoring the hydrolysis of synthetic peptide substrates at 410 nm as previously described (*22*, *26*). Values of $k_{cat}/K_m$ were determined as a function of viscosity at pH 9.0, 20 mM ethylenediamine buffer at 25 °C, and ionic strength 0.05 M (KCl) with glycerol as the viscosogenic agent (*27*).

## RESULTS

The enzyme-catalyzed hydrolysis of tetrapeptide substrates succinyl- and acetyl-AAPF-anilides was measured with a series of subtilisin variants by introducing remote charges spanning the surface of the enzyme to alter the $pK_a$ of the active site histidine. A previously engineered variant of *B. lentus* subtilisin with increased enzymatic activity, N76D/N87S/S103A/V104I (DSAI) (*9*), served as the parent sequence for all of the subtilisin variants described here.

The pH rate profiles for $k_{cat}/K_m$ are illustrated in Figure 1 for DSAI and a variant S166D. The data were fit to a two state ionization model as described in the Experimental Procedures. The unit slope at acidic pH is consistent with the ionization of a single acid group, assigned to the $pK_a$ ($N^{\epsilon 2}$-H) of the active site histidine-64 (*23*, *28*). The pH dependence of $k_{cat}/K_m$ gives ionization constants for the free enzyme, under conditions where the substrate does not ionize. Data are summarized in Table 1 for negatively charged

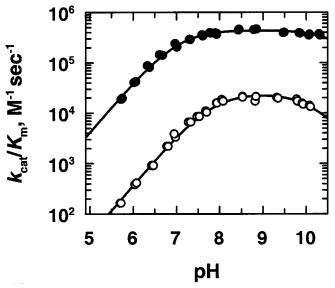


FIGURE 1: pH dependence of the second-order rate constants $k_{cat}/K_m$ for hydrolysis of suc-AAPF-pNA by DSAI (●; $pK_{a1} = 7.13$) and the S166D (○; $pK_{a1} = 7.66$) variant at ionic strength 0.05 M. Data were fit to a two state ionization model with $pK_{a1}$ corresponding to ionization of the active site His-64 $N^{\epsilon 2}$-H and $pK_{a2}$ corresponding to ionization of Y167 (B. Domingo and C. J. Murray, unpublished work).

(succinyl) and uncharged ac-AAPF-*p*NA substrates. There is no significant difference in the $pK_a$ determined with the two different substrates.

Previous work has shown that steric, hydrophobic, and electrostatic effects of residues at positions 156 and 166 in subtilisin BPN′ can modulate specificity for the hydrolysis of substrates at the $P_1$ position (*17*, *22*, *29*). For example, a plot of log $k_{cat}/K_m$ for hydrolysis of suc-AAPY-*p*NA versus side chain molecular volume for amino acid substitutions at position 166 in subtilisin BPN′ shows a linear relationship (slope = −0.02 log($k_{cat}/K_m$)/Å$^3$) (*17*) and indicates that a small steric factor is important for determining substrate hydrolysis rates for substitutions at position 166. Thus, $k_{cat}/K_m$ values for the S166D and S156E/S166D variants were corrected by a factor of 3 ($\Delta k_{cat}/K_m = 10^{(0.02)22}$) based on the 22 Å$^3$ difference in molecular volume between serine and aspartic acid side chains (*30*).[3]

To determine the dependence of the reaction rate on the $pK_a$ of the amine leaving group, a series of competitive kinetic experiments with substituted ac-AAPF-anilides were carried out to simultaneously monitor the hydrolysis of both substrates. The advantage of this approach is that very accurate relative second-order rate constants can be determined for several variants simultaneously in a 96-well plate format.

Figure 2 shows the competitive kinetics of the hydrolysis of pairs of ac-AAPF-anilide/*p*-nitroanilide substrates monitored under $k_{cat}/K_m$ conditions at pH 8.8 at 250 nm where the increase in absorbance ($\tau_1$) corresponds to the hydrolysis of the *p*-nitroanilide substrate, and the decrease in absorbance ($\tau_2$) corresponds to the hydrolysis of ac-AAPF-aniline. Relative rate constants $(k_{cat}/K_m)^{NO_2}/(k_{cat}/K_m)^H = \tau_2/\tau_1$ for *p*-nitroaniline and aniline leaving groups determined by this method are summarized in Table 1.

The normalized values for $(k_{cat}/K_m)_1$ are plotted versus relative viscosity in Figure 3 for DSAI and the S166D variant. The data show no significant change in the second-order rate constant with viscosity in glycerol−water mixtures.

Individual kinetic constants $k_{cat}$ and $K_m$, as well as inhibition constants $K_i$ for *Z*-LLF-$CF_3$, were determined for

[3] Similar analyses of substitutions at position 156 in subtilisin BPN′ and position 217 in subtilisin from *B. lentus* that line the $S_1$ and $S_1'$ subsites, respectively, show little evidence of significant steric effects (T. Graycar, unpublished results), so no correction was made for substitutions at these residues.

Table 1: Kinetic Analysis of *B. lentus* Subtilisin Variants for Hydrolysis of Ala-Ala-Pro-Phe Anilide Substrates[a]

| | Suc-AAPF-pNA | | Ac-AAPF-pNA | | Ac-AAPF-pNA/ Ac-AAPF-anilide[b] |
|---|---|---|---|---|---|
| variant | p$K_a$ H64 | $10^{-5}(k_{cat}/K_m)_1$ ($M^{-1}$ $s^{-1}$) | p$K_a$ H64 | $10^{-5}(k_{cat}/K_m)_1$ ($M^{-1}$ $s^{-1}$) | $(k_{cat}/K_m)^{NO_2}/(k_{cat}/K_m)^H$ |
| parent, DSAI | 7.13 | 3.0 (2.1)[c] | 7.16 | 2.2 | 5.1 |
| A98E | 7.28 | 2.4 | | | |
| S99D | 7.26 | 2.3 | 7.24 | 2.1 | 4.5 |
| S99K | 7.07 | 3.1 | | | |
| Q109R | | | 7.10 | 2.6 | |
| Q109E | | | 7.32 | 1.5 | |
| S156E | 7.33 | 1.9 | 7.41 | 1.3 | 6.2 |
| S156K | 7.05 | 3.3 | 6.98 | 1.9 | |
| G159D | 7.15 | 1.8 | | | |
| S166D | 7.66 | 0.23 (0.69)[d] | 7.82 | 0.22 (0.69)[c] | 7.7 |
| S156E/S166D | 7.82 | 0.075 (0.22)[d] | | | 10.4 |
| R170E | 7.25 | 1.8 | 7.25 | 1.0 | |
| G159D/Q206E | 7.25 | 1.9 | | | |
| Q206E | 7.13 | 3.0 | | | |
| Y209L | 7.11 | 3.0 | | | 4.8 |
| Y209D | 7.31 | 2.1 | 7.38 | 1.4 | 7.4 |
| Y209E | | | 7.30 | 1.7 | |
| L217E | 8.0[e] | 0.24 | | | 13.0 |
| S156E/L217E | 7.8[e] | 0.40 | 7.8[e] | 0.18 | |

[a] Kinetic constants at 25 °C, 0.05 M ionic strength were determined from pH rate profiles under pseudo-first-order conditions. Errors were typically less than ±0.04 p$K$ units for p$K_a$ values and less than 10% for $(k_{cat}/K_m)_1$. [b] Ratios of second-order rate constants were determined at pH 8.8, under competitive conditions ([S] ≪ $K_m$) as described in the Experimental Procedures. [c] Second-order rate constant in $D_2O$. [d] Corrected for a 3-fold steric effect at position 166 as described in the Results. [e] The pH rate profiles for L217E variants were fit to a two state Adair equation to account for the effect of ionization of E217 and H64 on $k_{cat}/K_m$. The corresponding errors are larger: ±0.1 p$K$ units.

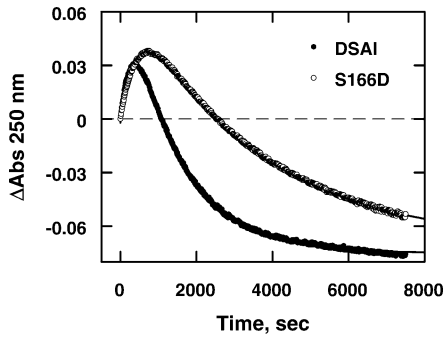


FIGURE 2: Kinetic time courses for the competitive hydrolysis of ac-AAPF-pNA ($1/\tau_1$) and ac-AAPF-anilide ($1/\tau_2$) by DSAI ($\tau_2/\tau_1 = 5.10 \pm 0.01$) and S166D ($\tau_2/\tau_1 = 7.69 \pm 0.02$).

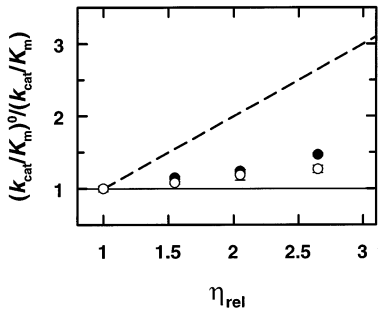


FIGURE 3: Viscosity dependence of $k_{cat}/K_m$ for DSAI (●) and S166D (○) in glycerol water at pH 9.0, at 25 °C, ionic strength 0.05 M (KCl). The dashed line corresponds to the limiting slope for a fully diffusion-controlled reaction.

a few variants by initial rate measurements and progress curve kinetics and are summarized in Table 2.

## DISCUSSION

Serine protease catalysis proceeds in three steps (Scheme 2), with acylation of the active site serine and release of the amine leaving group rate-determining for hydrolysis of amide substrates.

Table 2: Kinetic Analysis of Subtilisin Variants for Hydrolysis of Ac-Ala-Ala-Pro-Phe *p*-Nitroanilide and Inhibition by *Z*-Leu-Leu-Phe-Trifluoromethyl Ketone[a]

| | Ac-AAPF-pNA | | | *Z*-LLF-$CF_3$ |
|---|---|---|---|---|
| variant | $k_{cat}$ ($s^{-1}$) | $K_m$ (mM) | $10^{-5}k_{cat}/K_m$ ($M^{-1}$ $s^{-1}$) | $K_i$ (nM) |
| parent, DSAI | 220 | 1.9 | 1.2 | 18 |
| S99R/N204T | 294 | 1.8 | 1.6 | - |
| S156E | 200 | 3.4 | 0.58 | 57 |
| S166D | 33 | 3.3 | 0.11 | 460 |
| S156E/S166D | 9 | 4 | 0.02 | 2100 |

[a] Kinetic constants at 25 °C, pH 7.5, 50 mM potassium phosphate, and 4% DMSO were determined from initial rate measurements as described in the Experimental Procedures section. Errors were typically less than ±10%.

Scheme 2

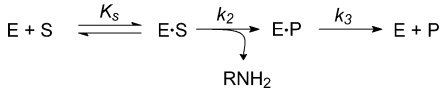


The absence of a pre-steady-state burst upon the hydrolysis of ac-AAPF-*p*NA by *B. lentus* subtilisin is consistent with rate-determining acylation with this substrate (*21*). There is no significant change in $k_{cat}/K_m$ with viscosity (Figure 3), indicating that the observed kinetic parameter $k_{cat}/K_m$ largely reflects rate-limiting chemical, rather than diffusive, steps for the enzyme variants reported here. The data in Table 2 show that there is only a small variation in $K_m$ for these variants (*31*) and suggests that the variations in $k_{cat}/K_m$ for tetrapeptide anilide substrates are dominated by transition state effects and not ground-state binding effects in the Michaelis E·S complex in Scheme 2. Finally, extensive work by others with the more commonly studied subtilisin BPN′

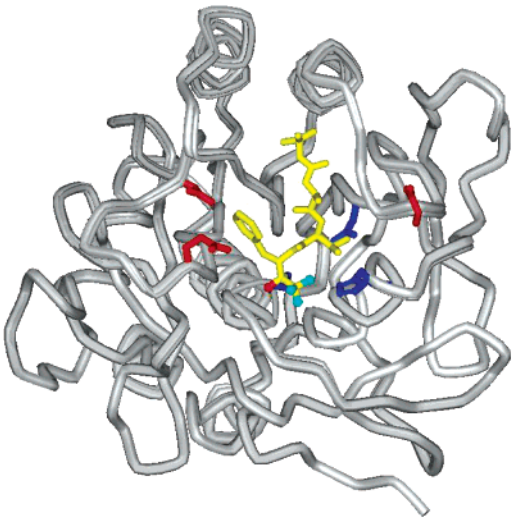

FIGURE 4: C-α aligned X-ray crystal structures of DSAI (PDB code 1C9M), S156E/S166D variant at 1.6 Å resolution, and a model of a transition state analogue inhibitor, *t*-butoxy-Ala-Leu-Phe-trifluoromethyl ketone bound to the active site Ser 221 of subtilisin BPN′ 8350 (PDB code 1S01) showing the location of charged amino acids D99, E156, and D166 in red. The active site residues are shown in blue, the inhibitor is shown in yellow with fluorine atoms in light blue, and the hemiketal oxyanion is in red. The distance between the Oδ1 of D166 and the oxyanion of the bound inhibitor is 8.3 Å.

enzyme and its variants (*2*, *17*, *26*, *27*, *31*, *32*) also supports the conclusion that acylation is the rate-determining step for the hydrolysis of tetrapeptide anilide substrates by subtilisin proteases.

Because of synergistic interactions between the $S_4$ and $S_1$ subsites (*22*, *33*, *34*), full utilization of the intrinsic binding energy of enzyme−substrate interactions requires occupancy of the $S_4-S_1$ specificity pockets by $P_4-P_1$ substrates that form a well-defined antiparallel $\beta$ sheet structure with the enzyme (Figure 4). Thus, interpretations of transition state structure using these small substrates are relevant to the physiological substrates used by these enzymes.

The enzyme substitutions reported here are unlikely to give rise to artifacts arising from large conformational changes. The substitutions generally line the surface of the enzyme near the active site, and many of the substitutions are observed in natural homologues (*23*, *35*, *36*). The substitutions make only small perturbations in enzyme structure (R. R. Bott, unpublished results (*8*)). For example, as illustrated in Figure 4, the C-α aligned X-ray crystal structures for DSAI and the S156E/S166D variant with the active site Ser-221 labeled with a phenylmethyl sulfonyl (PMS) group gave a root-mean-square deviation of 0.44 Å.

The conformation of the phenyl ring of the PMS group is oriented toward the $S_1$ subsite in the S156E/S166D variant, as shown in detail in Figure 5. The phenyl ring is 7.2 Å from the 156E side chain carboxyl, while the 166D side chain is 3.9 Å from the PMS group. The PMS group has an occupancy of less than 1.0, consistent with a large degree of conformational flexibility of the PMS group. Subtilisin variants with mutations in the $S_1$ subsite (including S166D) show a linear relationship between log $k_2/K_i$ for PMSF inactivation and log $k_{cat}/K_m$ for the hydrolysis of suc-AAPF-*p*NA, with a slope $\beta = 0.6$ (C. Y. Hsia and C. J. Murray, unpublished work). This suggests that the orientation of the phenyl ring in the PMSF inhibited S156E/S166D structure

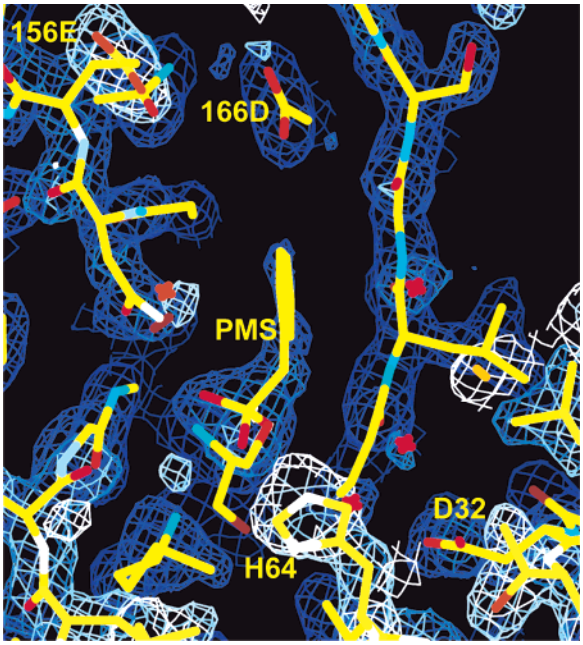


FIGURE 5: Phenylmethyl-sulfonyl (PMS) group interacting with the S156E/S166D side chains showing $2F_0 - F_c$ electron density map at 1.6 Å resolution contoured at 1$\sigma$. The active site residues D32 and H64 are shown along with the PMS-S221 residue.

Scheme 3

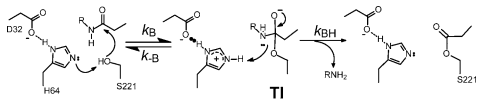


mimics the orientation of the substrate phenylalanyl side chain in the transition state and that variations in structure around the active site are not affected by the ability of charged mutations to change hydrogen bond donors and acceptors. This conclusion is also consistent with the modeled structure of the peptidyl trifluoromethyl hemiketal shown in Figure 4 as well as with the small 3-fold steric effect on $k_{cat}/K_m$ for the S166D variants. We conclude that the variations in enzyme properties introduced by these mutations are global properties of the protein.

*Nature of the Rate-Determining Step for Acylation.* The function of the serine in the rate-determining acylation step of serine protease catalysis is to enter into a transacylation reaction with the amide substrate to form an acyl−enzyme intermediate E·P in Scheme 3.

The role of the imidazole $N^{\epsilon 2}$ of His-64 is to act as a general base catalyst to assist the nucleophilic attack of the serine oxygen ($k_B$), while the imidazolium form acts as a general acid to facilitate amine expulsion ($k_{BH}$) from the tetrahedral intermediate (TI). Within the overall acylation step, tetrahedral adduct formation ($k_B$) or breakdown ($k_{BH}$) may be rate-limiting (*3*, *37*). Early mechanistic experiments with serine proteases using isotope effects and structure−reactivity correlations have been interpreted in terms of both rate-limiting tetrahedral adduct formation and breakdown (*37*−*39*).[4] Rate-limiting TI formation is consistent with the

[4] Much of the early work on the analysis of transition state structure in serine protease catalysis refers to small substrates binding in the $S_1$ or $S_2-S_1$ subsites only.

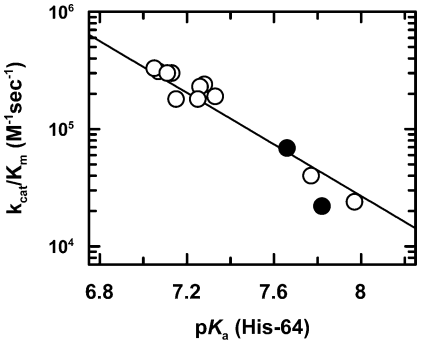


FIGURE 6: Brønsted plot for general acid catalysis of the hydrolysis of suc-AAPF-pNA by subtilisin variants at 25 °C and ionic strength 0.05 M. The line corresponds to a Brønsted slope $\alpha = 1.1 \pm 0.1$. The points for S166D and S156E/S166D variants (●) were corrected for a steric effect as described in Results.

increased basicity of His-64 $N^{\epsilon 2}$ upon the binding of peptidyl trifluoromethyl hemiketals that are transition state analogues (*20*) as well as the electrostatic stabilization of these bound inhibitors, analogous to the charge separated TI structure in Scheme 3 (*26*). However, at best these are analogues of the unstable tetrahedral intermediate. To the extent that the enzyme stabilizes this intermediate, the binding of the analogue will reflect the forces that increase the reaction rate but will not distinguish the nature of the rate-limiting step. In this context, the use of LFERs can provide a detailed description of the acid−base properties of the catalytic histidine in the transition state.

The data in Table 1 have been used to generate a linear free energy relationship (eq 1) between $\log(k_{cat}/K_m)$ and the p$K_a$ of the active site His-64 of subtilisin (Figure 6). The Brønsted plot for enzyme catalysis of the hydrolysis of suc-AAPF-pNA has a slope $\alpha = 1.1 \pm 0.1$. This slope is consistent with a transition state for breakdown of the tetrahedral intermediate involving partial carbon−nitrogen (C−N) bond cleavage that is stabilized by hydrogen bonding to the His-64 imidizolium $N^{\epsilon 2}$ nitrogen ($k_{BH}$ in Scheme 3 and the reverse reaction illustrated in Scheme 1). The Brønsted slope is inconsistent with an increase in the reaction rate with increased p$K_a$ expected for a general base-catalyzed reaction ($k_B$ in Scheme 3).

Further support for a mechanism involving stabilization of the departing amine by the catalytic His-64 is provided by the dependence of the reaction rate on the basicity of the amine leaving group and the solvent isotope effect $^{D_2O}(k_{cat}/K_m)_1 = 1.4 \pm 0.2$ for DSAI-catalyzed hydrolysis of suc-AAPF-*p*NA. Coupling of the proton transfer to motion of heavy atoms in the transition state is one of several explanations that can account for small deuterium isotope effects. An estimate of ∼20−40% C−N bond cleavage in the transition state can be obtained from $\beta_{lg}^n$ that describes the effect of changes in the basicity of the amine leaving group on reaction rate. Changes in the carbon−nitrogen bond order can be roughly quantitated according to eq 4

$$\beta_{lg}^n = \frac{\partial \log(k_{cat}/K_m)}{\partial pK_a^{lg}\beta_{eq}} \approx \frac{\Delta\log(k_{cat}/K_m)}{3 \times 0.7} \qquad (4)$$

based on the increased relative rate constant for *p*-nitroaniline versus aniline leaving groups ($(k_{cat}/K_m)^{NO_2}/(k_{cat}/K_m)^{H}$; Table 1), the ∼3 unit difference in p$K_a$ for *p*-nitroaniline versus aniline (*40*), and a value of $\beta_{eq} = \partial \log K/\partial pK_a = 0.7$ for equilibrium acyl transfer of substituted anilines with alkyl esters (*41*). We conclude that the rate-limiting step for hydrolysis of tetrapeptide anilide substrates (and presumably oligopeptide substrates as well) by *B. lentus* subtilisin is breakdown of the tetrahedral intermediate ($k_{BH}$ in Scheme 3).

The large value of α suggests that in the transition state, the His-64 imidazolium ion is largely positively charged with little proton transfer from the $N^{\epsilon 2}$-H to the amine leaving group, even though proton transfer to a partially negatively charged amine is expected to be thermodynamically favorable. There are several possible explanations for this apparent imbalance. (1) The Bronsted $\beta_{lg}^n$ may overestimate the degree of C−N bond cleavage due to the inability of the para-nitro group to delocalize the partial charge on the amine nitrogen effectively in the enzyme active site, relative to ionization of substituted anilines in water (*40*). (2) The Bronsted α may overestimate the degree of proton transfer in the transition state due to electrostatic destabilization of the transition state. (3) Hydrogen bonding of the imidizolium ion $N^{\epsilon 2}$—H···N hydrogen bond may be particularly strong in the low dielectric environment of the enzyme active site, relative to hydrogen bonds in water. These latter two explanations are discussed in more detail below, but all of these possibilities point to the difficulties in interpreting structure−reactivity relationships for enzymes where the ground-state reference reactions involve the ionization of acids and bases in water, in the absence of the enzyme.

*Consequences of Electrostatic Effects on Brønsted Slopes in Enzyme Reactions.* LFERs assume that transition state properties such as charge development or changes in bond order (see Scheme 1) are intermediate between reactants and products (*19*, *41*). Charge development and the value of α in eq 1 may be related to bond orders if only one bond is made or broken. However, for the multiple bond forming reactions, Brønsted slopes may be affected by simple electrostatic effects that change the energy of the transition state, in the absence of any change in the structure of the transition state. The electronic rearrangements that occur upon formation and breakdown of the TI in Scheme 3 require large changes in charge density in going from the ground state to the transition state (*26*, *32*, *42*). Electrostatic interactions that are only expressed in the transition state (formation of the charge separated TI, for example) and not in the ground-state reference reaction (ionization of the His-64 $N^{\epsilon 2}$-H in the free enzyme in this case) may give rise to anomalously large Brønsted slopes $\alpha > 1$.

Warshel and Florian (*42*, *43*) have pointed out that the reorganization energy of orienting polar groups in an enzyme active site is small, relative to the reaction in solution, because the dipoles are already positioned to interact with the transition state. Changes in these dipoles by remote electrostatic interactions may affect ground states and transition states differently. This offers an alternative explanation for the large observed Brønsted slope. For example, increased charge−charge repulsion between the D166 residue that is 8.3 Å away from the TI oxyanion (Figure 4) should destabilize the charged TI and slow the reaction rate, corresponding to an increase in the observed Brønsted slope for negatively charged variants.

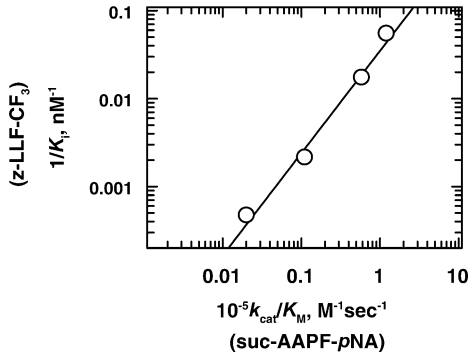


FIGURE 7: Comparison of the second-order rate constant for hydrolysis of suc-AAPF-pNA with the binding affinity of *Z*-LLF-trifluoromethyl ketone transition state analogue inhibitors for subtilisin variants at pH 7.5, 25 °C, and ionic strength 0.05 M. The line corresponds to a slope = 1.2 ± 0.1.

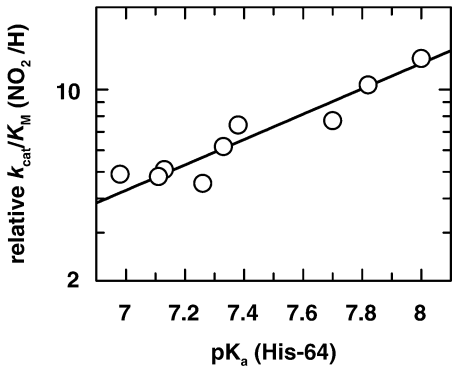


FIGURE 8: Dependence of the ratio of $k_{cat}/K_m$ for ac-AAPF-pNA and ac-AAPF-aniline on the p$K_a$ of His-64. The increase in relative rate constants for the two substrates corresponds to an increase in $\beta_{lg}$ with less acidic catalysts that can be described by the interaction coefficient $p_{xy} = \partial\beta_{lg}/\partial pK_a = 0.15$, calculated by dividing the observed slope of 0.46 ± 0.05 by $\Delta pK_a = 3$ corresponding to the difference in the p$K_a$ of the aniline leaving group.

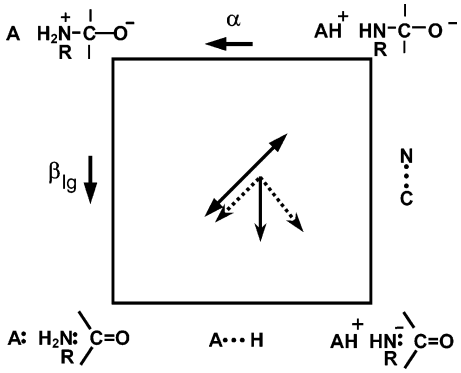


FIGURE 9: Reaction coordinate diagram for the general base-catalyzed addition of $RNH_2$ to the carbonyl group and the reverse, acid-catalyzed breakdown of the tetrahedral intermediate by a class *n* mechanism, after Jencks (*19*). The double-headed arrow represents the reaction coordinate. The dashed line illustrates the effect of increasing the basicity of the acid catalyst on the position of the transition state. The solid arrow is the result of those vectors.

It is difficult to parse the observed Brønsted slope into effects due to electrostatics on reaction rate and a true measure of proton transfer from the catalytic His-64 to the leaving group nitrogen in the transition state. However, there is some evidence to suggest that a differential expression of electrostatic effects in the ground and transition states cannot account for the large Brønsted slope in Figure 6. First, we note that the Brønsted slope for hydrolysis of the uncharged substrate Ac-AAPF-pNA ($\alpha = 1.1 \pm 0.3$; Table 1) is not significantly different from the slope for the charged substrate suc-AAPF-*p*NA determined with a more extensive set of variants. This is consistent with the small variation in $K_m$ for charged variants (Table 2) and suggests that any charge−charge interactions between the substrate and the enzyme in the ground state E·S complex are small. We therefore interpret the Brønsted slope as representing largely changes in charge developed in the transition state of the enzyme reaction. Second, as shown in Figure 7, for a series of charged variants there is a slightly larger decrease in the affinity for stable tetrahedral hemiketal adducts formed with *Z*-LLF-$CF_3$ relative to decreases in the corresponding reaction rate constant $k_{cat}/K_m$ (i.e., transition state affinity) corresponding to a slope of 1.2 ± 0.1. This suggests that electrostatic interaction effects that would be expected to give rise to $\alpha > 1$ in the partially charged transition state are less than in the stable hemiketal intermediate.

*Changes in Enzymatic Transition State Structure.* There is an increase in the amount of C−N bond cleavage with increasing p$K_a$ of the His-64 general acid catalyst (weaker acid) as illustrated in Figure 8. The increase in relative rate constants for the *p*-nitroaniline versus aniline leaving groups corresponds to an increase in $\beta_{lg}$ with weaker acid catalytic His-64 that can be described by the interaction coefficient $p_{xy}' = \partial\beta_{lg}/\partial pK_a = 0.15$.[5] There is a corresponding increase in the Brønsted α value for the more basic leaving group $p_{xy}' = \partial\alpha/\partial pK_{lg} = 0.2$ (data not shown) that partially reflects an electrostatic contribution to hydrogen bond formation as described below.

The changes in the Brønsted coefficient with reactant structure are consistent with a coupling between hydrogen bonding from the His-64 imidazolium ion with the change in bond order or charge on the central nitrogen of the amine leaving group in a concerted transition state for the breakdown of the TI. These changes can be described by the reaction coordinate diagram shown in Figure 9 for the general acid-catalyzed breakdown of the TI that corresponds to the reverse reaction shown in Scheme 1 (*19*).

The TI is shown in the upper right corner of the diagram. The catalyst $AH^+$ corresponds to the His-64 $N^{\epsilon 2}$-H. The acyl−enzyme intermediate is in the lower left-hand corner. The horizontal axis is defined by the Brønsted α representing proton transfer and the vertical axis by $\beta_{lg}$ for C−N bond cleavage. The values of α and $\beta_{lg}$ define the range of movement of the transition state with changes in p$K_a$ of the enzyme catalyst and substrate leaving group, respectively. The diagram provides a convenient way to visualize changes in the transition state structure in terms of experimentally observed LFER parameters.

The observed changes in Brønsted slopes indicate that as the basicity of the catalyst increases, there is more weakening of the bond to the leaving group nitrogen in the transition state for breakdown of the TI, $k_{BH}$ in Scheme 3. For a diagonal reaction coordinate through the center of the diagram,[6] a change to a more basic catalyst (A: = His-64

[5] A similar increase in the ratio of $k_{cat}/K_m$ for the *p*-nitroaniline vs the 3-fluoroaniline leaving group is observed as well (C. J. Murray, unpublished work).

N$^{\epsilon 2}$) will decrease the stability of the intermediates on the left side of the diagram. This will shift the transition state parallel and perpendicular to the reaction coordinate as illustrated by the dashed lines in Figure 9. The shift results in an increase in the amount of C−N bond cleavage, as measured by an increase in $\beta_{lg}$ (Figure 6). Although the analysis presented here is certainly an oversimplification, it nevertheless provides a description of the transition state that will not be altered greatly by large uncertainties in the structure−reactivity coefficients and is consistent with the experimental data.

*Do Enzymes Change the Nature of Transition States from those Observed in Solution?* The changes in the transition state structure with a changing enzyme acid−base catalyst and substrate leaving group reported here are larger than for comparable acyl transfer reactions involving acid−base catalysis of charge reorganization in water. The most directly comparable nonenzymatic reactions correspond to the general base-catalyzed aminolysis of esters (*37*, *44*). These reactions proceed in the reverse direction, via the zwitterionic tetrahedral intermediate, shown in the upper left-hand corner in Figure 9, because the intermediate has a significant lifetime in water. This corresponds to $p_{xy}' = 0$ and diffusion steps become rate-limiting (*44*). Jencks (*19*) has reported several examples of acyl transfer reactions that proceed via concerted reaction mechanisms that are generally described by much smaller interaction coefficients $\partial\beta_{lg}/\partial pK_a = \partial\alpha/\partial pK_{lg} \leq 0.06$ that describe the strength of coupling between proton transfer to electronegative atoms and heavy-atom reorganization in water (*4*).

It is not clear whether the observed changes in structure−reactivity parameters generated by remote electrostatic effects on an enzyme can be compared to changes in reactivity induced by through-bond dipole−dipole interactions of acids and bases in aqueous solution (*45*). The site-directed mutation of residues that lie close to the active site catalytic residue may be similar conceptually to changes in the reactivity of a catalyst introduced by changing solvents (*15*), rather than simple dipole−dipole interactions introduced by changing substituents in a catalyst. Further experimental and computational work will be needed to evaluate the significance of such changes in reactivity on enzyme transition state structure (*13*).

*Changes in Hydrogen Bond Strength in the Active Site of Enzymes. Application of the Hine Equation.* Since the rate-limiting step for serine protease catalysis involves hydrogen bond stabilization of the leaving group nitrogen by the active site histidine, it is appropriate to ask the question of whether the transition state hydrogen bond illustrated in Scheme 1 shares any properties with hydrogen bonds between solutes in water (*46*). It has been proposed that the sensitivity or change in hydrogen bond strength for enzymatic catalysis might be larger than changes in hydrogen bond strength for normal acids and bases in water (*47*). This proposal is supported by the observation of larger Brønsted slopes in organic solvents (*48*) as a crude model of the low effective dielectric of an enzyme active site. For a hydrogen bonded A−H···:B pair, there is an increase in hydrogen bond strength that accompanies an increase in partial charge density on the acceptor :B (as measured by a larger Brønsted slope $\alpha = \partial \log K_{AH\bullet B}/\partial pK_{AH}$ for a more basic acceptor $pK_{BH}$). The interplay between hydrogen bond donor and acceptor characteristics can be described by the interaction coefficient $\tau$ (eq 5) that describes changes in the strength of a hydrogen bond with changes in the $pK_a$ of the proton donor and acceptor according to the electrostatic model of hydrogen bonding proposed by Hine (*46*−*49*).

$$\tau = \frac{\partial\alpha}{\partial pK_{BH}} = \frac{\partial\beta}{\partial pK_{AH}} \qquad (5)$$

As illustrated in Scheme 1 for transition state hydrogen bonding between an enzyme catalyst and the leaving group amine, for an active site general acid AH to provide a catalytic advantage relative to water in the transition state, there must be an increase in the interaction coefficient $\tau$ that describes the strength of the hydrogen bond interaction $K_{AB}$ with changes in the $pK_{AH}$ of the acid catalyst and $pK_a$ of the leaving group nitrogen ($pK_{BH}$) in the transition state. A value for the hydrogen bond interaction coefficient $\tau \geq 0.06$ is required to account for the observed catalysis by a hydrogen bonding mechanism.[7] This is consistent with the observed $p_{xy}' = \partial\alpha/\partial pK_{lg}$ and is substantially larger than values of $\tau < 0.016$ for hydrogen bond interactions between normal acids and bases in water (*47*) or organic solvents (*48*).

The A···H···N hydrogen bond in the transition state of Scheme 1 might be compressed, relative to the ground state, such that there is little, if any, barrier for motion across the hydrogen bond (*4*). This is consistent with the small solvent isotope effect on $k_{cat}/K_m$ as well as with an increase in the value of $\tau$ that is required for a symmetrically hydrogen bonded proton with no barrier for motion of the proton as originally proposed by Hine (*49*).

## ACKNOWLEDGMENT

We thank J. P. Richard, C. F. Bernasconi, R. Schowen, and C. Holman for helpful discussions and T. Graycar and C. Whitlow for permission to cite unpublished work.

[6] Because of uncertainties in the degree of proton transfer (*vida supra*), the central transition state is presented for illustration purposes only. The data are equally consistent with a constant C− N bond order, with the proton moving closer to the more basic His (a purely perpendicular effect) or a constant His−HN bond order, with a decrease in the C−N bond order as the His becomes more basic (parallel effect). Perpendicular, or anti-Hammond, effects represent movement toward the more stable intermediate, and parallel, or Hammond, effects represent movement away from the more stable intermediate. The amount of the movements depends on the magnitude and sign of the curvatures perpendicular and parallel to the reaction coordinate.

[7] This estimate is based on a modified form of the Hine equation (*47*): $\log K_{AHB} = \tau(pK_a^{H_3O^+} - pK_a^{BH})(pK_a^{AH} - pK_a^{H_2O}) - \log(2 \times 55)$ The value of $\tau \geq 0.06$ was calculated from this equation using the upper limit for the $pK_a^{BH} = 18.4$ (*40*) of the transition state assuming a full negative charge buildup on the leaving group nitrogen, a value of $pK_a^{AH} = 10$ for the active site His-64 with the TI bound (*20*), and a value of $K_{AB} = 5 \times 10^4$ based on the decrease in $k_{cat}/K_m$ for the hydrolysis of suc-AAPF-*p*NA by an H64A variant of subtilisin BPN′ (*50*). This calculation yields a lower limit for the value of $\tau$ because the $pK_a^{BH}$ of the transition state will be smaller due to partial bonding between the central carbon and the leaving group nitrogen. We note that the proposal by Shan and Herschlag (*47*) for an increased strengthening of the hydrogen bond in a nonaqeous enzymatic active site relative to a hydrogen bond in water that corresponds to an increase in Brønsted slope, $\Delta\beta^{soln\rightarrow E}$, requires a corresponding increase in the hydrogen bond interaction coefficient according to $\Delta\beta = \Delta\tau(pK_{HA} - pK_{HOH})$ (*47*). Thus, large interaction coefficients may be a fundamental requirement for acid−base catalysis in enzyme active sites.

## REFERENCES


1. Fischer, E. (1894) *Ber. Dtsch. Chem. Ges. 27*, 2985.
2. Polgar, L., and Bender, M. L. (1969) *Proc. Natl. Acad. Sci. U.S.A. 64*, 1335−42.
3. Fersht, A. (1985) *Enzyme Structure and Mechanism*, 2nd ed., W. H. Freeman and Co., New York.
4. Schowen, K. B., Limbach, H. H., Denisov, G. S., and Schowen, R. L. (2000) *Biochim. Biophys. Acta 1458*, 43−62.
5. Albery, W. J., and Knowles, J. R. (1976) *Biochemistry 15*, 5627−31.
6. Toney, M. D., and Kirsch, J. F. (1989) *Science 243*, 1485−8.
7. Richard, J. P. (1998) *Biochemistry 37*, 4305−9.
8. Mulder, F. A., Schipper, D., Bott, R., and Boelens, R. (1999) *J. Mol. Biol. 292*, 111−23.
9. Graycar, T., Knapp, M., Ganshaw, G., Dauberman, J., and Bott, R. (1999) *J. Mol. Biol. 292*, 97−109.
10. Kuhn, P., Knapp, M., Soltis, S. M., Ganshaw, G., Thoene, M., and Bott, R. (1998) *Biochemistry 37*, 13446−52.
11. Alston, W. C., II, Kanska, M., and Murray, C. J. (1996) *Biochemistry 35*, 12873−81.
12. Alston, W. C., II, Haley, K., Kanski, R., Murray, C. J., and Pranata, J. (1996) *J. Am. Chem. Soc. 118*, 6562−9.
13. Kraut, D. A., Carroll, K. S., and Herschlag, D. (2003) *Annu. Rev. Biochem. 72*, 517−571.
14. Brønsted, J., and Pedersen, K. (1924) *Z. Phys. Chem. 108*, 185.
15. Bell, R. (1958) *The Proton in Chemistry*, Chapman and Hall, London.
16. Admiraal, S. J., Meyer, P., Schneider, B., Deville-Bonne, D., Janin, J., and Herschlag, D. (2001) *Biochemistry 40*, 403−13.
17. Estell, D. A., Graycar, T. P., Miller, J. V., Powers, D. B., Burnier, J. P., Ng, P. G., and Wells, J. A. (1986) *Science 233*, 659−63.
18. Estell, D. A. (1987) *Protein Eng. 1*, 445−6.
19. Jencks, W. (1985) *Chem. Rev. 85*, 511−27.
20. Halkides, C. J., Wu, Y. Q., and Murray, C. J. (1996) *Biochemistry 35*, 15941−8.
21. Hsia, C. Y., Ganshaw, G., Paech, C., and Murray, C. J. (1996) *Anal. Biochem. 242*, 221−7.
22. Ballinger, M. D., Tom, J., and Wells, J. A. (1996) *Biochemistry 35*, 13579−85.
23. Russell, A. J., Thomas, P. G., and Fersht, A. R. (1987) *J. Mol. Biol. 193*, 803−13.
24. Leatherbarrow, R. J. (1998) *Grafit version 3.0*, Erithacus Software Ltd., Staines, UK.
25. Bernasconi, C. (1976) *Relaxation Kinetics*, Academic Press, New York.
26. Jackson, S. E., and Fersht, A. R. (1993) *Biochemistry 32*, 13909−16.
27. Stratton, J. R., Pelton, J. G., and Kirsch, J. F. (2001) *Biochemistry 40*, 10411−6.
28. Day, R. M., Thalhauser, C. J., Sudmeier, J. L., Vincent, M. P., Torchilin, E. V., Sanford, D. G., Bachovchin, C. W., and Bachovchin, W. W. (2003) *Protein Sci. 12*, 794−810.
29. Wells, J. A., Powers, D. B., Bott, R. R., Graycar, T. P., and Estell, D. A. (1987) *Proc. Natl. Acad. Sci. U.S.A. 84*, 1219−23.
30. Chothia, C. (1975) *Nature 254*, 304−8.
31. Philipp, M., and Bender, M. L. (1983) *Mol. Cell Biochem. 51*, 5−32.
32. Wells, J. A., Cunningham, B. C., Graycar, T. P., and Estell, D. A. (1986) *Philos. Trans. R. Soc. London Ser. A 317*, 415−23.
33. Gron, H., and Breddam, K. (1992) *Biochemistry 31*, 8967−71.
34. Rheinnecker, M., Baker, G., Eder, J., and Fersht, A. R. (1993) *Biochemistry 32*, 1199−203.
35. Loewenthal, R., Sancho, J., Reinikainen, T., and Fersht, A. R. (1993) *J. Mol. Biol. 232*, 574−83.
36. Siezen, R. J., de Vos, W. M., Leunissen, J. A., and Dijkstra, B. W. (1991) *Protein Eng. 4*, 719−37.
37. Satterthwait, A. C., and Jencks, W. P. (1974) *J. Am. Chem. Soc. 96*, 7018−31.
38. Hiroara, H., Bender, M. L., and Stark, R. S. (1974) *Proc. Natl. Acad. Sci. U.S.A. 71*, 1643−7.
39. Hegazi, M. F., Quinn, D. M., and Schowen, R. L. (1976) in *Transition States of Biochemical Processes* (Gandour, R. D., and Schowen, R. L., Eds.) pp 355−423, Plenum Press, New York.
40. Stewart, R., and O'Donnell, J. P. (1962) *J. Am. Chem. Soc. 84*, 493−4.
41. Williams, A. (1992) *Adv. Phys. Org. Chem 27*, 1−55.
42. Warshel, A. (1998) *J. Biol. Chem. 273*, 27035−8.
43. Warshel, A., and Florian, J. (1998) *Proc. Natl. Acad. Sci. U.S.A. 95*, 5950−5.
44. Yang, C. C., and Jencks, W. P. (1988) *J. Am. Chem. Soc. 110*, 2972−3.
45. Hine, J. (1959) *J. Am. Chem. Soc. 81*, 1126−1129.
46. Stahl, N., and Jencks, W. P. (1986) *J. Am. Chem. Soc. 108*, 4196−205.
47. Shan, S. O., and Herschlag, D. (1999) *Methods Enzymol. 308*, 246−76.
48. Coleman, C. A., and Murray, C. J. (1992) *J. Org. Chem. 57*, 3578−82.
49. Hine, J. (1972) *J. Am. Chem. Soc. 94*, 5766−71.
50. Carter, P., and Wells, J. A. (1988) *Nature 332*, 564−8.


BI034773M